Friction

Research Article

From sparks to wear: Understanding arc erosion and tribological mechanisms in pantograph-catenary systems under irregular wire conditions

Dehui Ji[1], Siyang Chen[1], Haihong Wu[2], Guoliang Wu[2], Minhao Zhu[3], Mingxue Shen[1,✉]

Cite this article: Ji DH, Chen SY, Wu HY, et al. *Friction* 2026, **14**(3): 9441102. https://doi.org/10.26599/FRICT.2025.9441102

ABSTRACT: The pantograph-catenary system bears the crucial task of supplying electrical energy to high-speed trains. However, as train speeds continue to increase, irregularities in the contact wire exacerbate vibrations within the pantograph-catenary system, frequently triggering pantograph arcs. To delve deeper into the characteristics and erosion mechanisms of these arcs, this study employed high-speed cameras and photodiodes to precisely capture the evolution of the arc morphology and fluctuations in the arc intensity triggered by contact pair irregularities. By adjusting the current intensity, we further analyzed the impact of arc discharge on the friction and wear performance of the carbon strips, as well as their current-carrying efficiency. The study revealed that when the current is sufficiently high, the arc column of the old arc, which forms when the contact pair separates, connects with the arc root of the new arc that is yet to make contact, leading to the formation of a continuous arc. Additionally, under the same current conditions, the arc intensity prior to contact between tribo-pairs is notably weaker than that at the moment of separation. Furthermore, parameters such as the arc ignition rate, wear volume, and temperature are positively correlated with the current intensity. Severe arc discharge not only deteriorates the electrical performance of the system, causing current distortion, but also exacerbates the instability of system operation. Abrupt changes in the friction coefficient can serve as harbors of intense arcs between the contact pair. Arc erosion causes severe damage to current-carrying tribo-pairs, with ablation pits eliminating thermal cracks and pores and leaving behind numerous molten copper particles, significantly increasing the wear volume. This study provides strong support for understanding the arc erosion process caused by contact wire irregularities and the mechanisms underlying the abnormal wear of carbon strips.

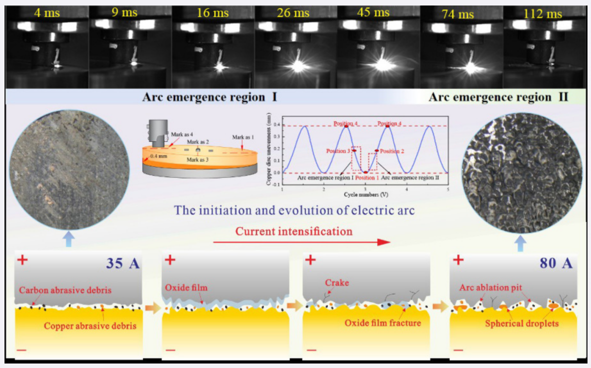

KEYWORDS: pantograph-catenary system; current intensity; irregularity; current-carrying friction; C/Cu; arc erosion

1 Introduction

The pantograph-catenary system provides energy for training via the sliding contact between the contact wire and the carbon strips. Ensuring the optimal state of this contact is vital for the safe and reliable operation of high-speed railways, which has garnered considerable attention from researchers globally [1, 2]. Nevertheless, as train speeds increase, the vibrations of both the pantograph carbon strips and the contact wire intensify, resulting in frequent pantograph arc occurrences [3]. The severe erosion effect stemming from arc discharge causes considerable wear on the carbon strips, thereby posing a significant threat to their durability.

With respect to the sliding contact of the pantograph-catenary system, numerous previous studies have explored the impact of various experimental conditions on the tribological and wear performance, as well as the current-carrying capacity, of the contact pairs [3–6]. Guo et al. [7] reported that the friction coefficient and wear rate between carbon strips and contact wires are related to the intensity of arc discharge. They noted that the friction coefficient under no-current conditions is significantly greater than that under current-carrying conditions and decreases as the current increases [8]. However, an increase in arc discharge leads to exacerbated material wear [9]. Subsequent in-depth research on current-carrying friction in pantograph-catenary systems revealed that the wear mechanism of the system varies

[1] State Key Laboratory of Performance Monitoring and Protecting of Rail Transit Infrastructure, East China Jiaotong University, Nanchang 330013, China. [2] CSSC Jiangxi Jiujiang Marine Equipment Co., Ltd., Jiujiang 332008, China. [3] Southwest Jiaotong University, Chengdu 611756, China.

✉ Corresponding author. E-mail: shenmingxue@126.com

Received: December 8, 2024; Revised: February 15, 2025; Accepted: March 22, 2025

with changes in current. An increase in current causes surface damage to transition from adhesive and mild abrasive wear to delamination and electrical wear [10]. Mei et al. [11] reported that the wear of carbon strips primarily consists of electrical wear and mechanical wear, with the duration of discharge arcs in electrical wear closely related to material damage [12]. These studies collectively indicate that, with increasing current, electrochemical wear becomes the dominant wear mechanism at the current-carrier contact interface, whereas mechanical wear has a minimal impact. Among them, arc discharge is a key focus of electrochemical wear research [13, 14]. In addition to the impact of arc erosion on worn surfaces, researchers have investigated the movement patterns of arcs. Xu et al. [13] studied the movement forms of discharge arcs and observed two typical irregular arc motion phenomena: arc foot jumping and arc reignition. Factors such as the contact force, contact current, and contact materials corresponding to different operating states and train configurations have varying degrees of influence on the movement patterns of arcs [15, 16]. Luo et al. [17] experimentally reported that as the carbon strips move forward relative to the contact wire, the arc moves backward along the contact wire, thereby affecting system performance.

In summary, the characteristics and intensity of arc discharges are crucial for studying the wear mechanisms and electrical transmission performance of pantograph-catenary systems. The vertical vibrations of the pantograph and catenary [18–20], irregularities in the contact wire, and the presence of ablation-induced deposits or other impurities adhering to the catenary [21] can all cause varying degrees of off-line arc discharges. Among these factors, the occurrence of contact wire irregularities has multiple causes in actual railway lines [17], such as wear on the contact wire, hard spots, engineering errors during installation, and conductor height settlement. The irregularity of the contact surface is essentially a stochastic process arising from the superposition of random irregularities with varying wavelengths, phases, and amplitudes. However, for an infinitely long catenary system, this can be approximated as a stationary and ergodic stochastic process categorized into two types: periodic irregularity and random irregularity [22]. However, regardless of the cause, irregularities inevitably lead to separation within the pantograph-catenary system, resulting in frequent arc discharges. This not only degrades the current collection quality of trains but also erodes the pantograph-catenary system, causing frequent accidents. Research on contact wire irregularities has focused primarily on dynamic simulations and algorithm validation analysis, and there have been no reports on induced wear damage to carbon strips and arc discharge behavior. Furthermore, research on the correlation between varying arc intensities and the tribological properties and current-carrying capacity of carbon strips remains incomplete and lacks systematic investigation.

To further elucidate the erosion process and discharge behavior of arcs, this paper comprehensively investigates the tribological characteristics and evolution of the current-carrying capacity of carbon strips, focusing on the influence of arcs under the condition of contact wire irregularities by varying the current intensity. This investigation delves into the specific changes in the friction coefficient and wear volume of the contact interface across different current levels. The evolution characteristics and intensity changes of the arc shape caused by irregular contact pairs were recorded by high-speed cameras and photodiodes. Additionally, the macroscopic and microscopic morphologies of the carbon strips after arc erosion, in addition to their conductive properties, including the arc incidence rate and current-carrying efficiency of the contact interface, across various arc intensities were compared. This study establishes a clear correlation between the friction coefficient, instantaneous current, and arc intensity and formulates a functional relationship linking the arc energy to the temperature of the contact pairs. Ultimately, this research contributes to a better understanding of the arc erosion process and the abnormal wear mechanisms of carbon strips caused by contact wire irregularities.

2 Experimental

2.1 Experimental equipment and materials

The experiments were conducted on a self-assembled current-carrying pin-on-disk tribometer, and a schematic diagram of the tribometer is shown in Fig. 1(a). This tribometer can effectively simulate the high-speed sliding friction process under current-carrying conditions. A photodiode (S5971, Hamamatsu Photonics K.K., Japan) was used to detect the arc intensity in real time, whereas a high-speed camera (i-SPEED 717, iX Cameras Ltd., UK) captured and recorded the arc morphology at a frame rate of 1,000 frames per second to document the initiation, development, and extinction of the arc. A schematic diagram of the experimental circuit is depicted in Fig. 1(b), and the circuit consists of a voltage source, a relay, a current sensor, a resistor, a sample, and a voltage sensor. The voltage source can provide a stable direct current (DC) voltage ranging from 5 to 80 V. The current sensor and voltage sensor record the circuit current and the voltage between contact pairs in real time, respectively, and then transmit the data to a computer via a data acquisition unit.

The upper sample used in the current-carrying friction test was sourced from pure carbon strips currently in service on high-speed railways (with the sampling location shown in Fig. 1(c)). This material exhibits excellent mechanical and electrical

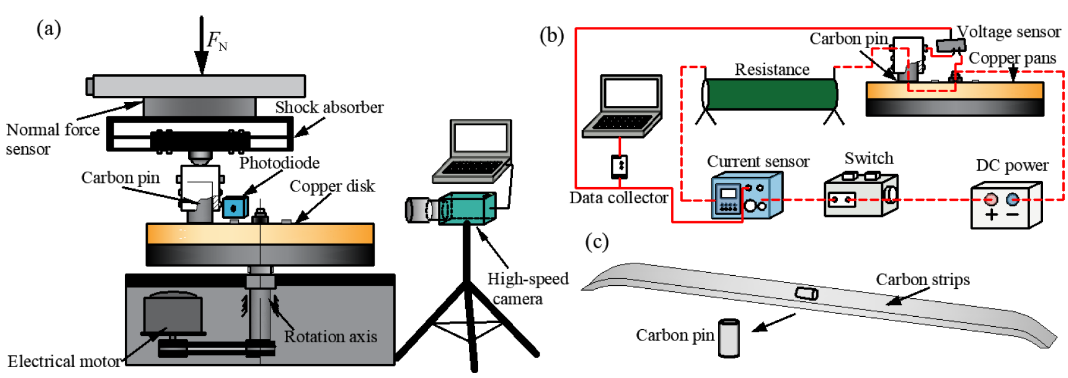

Fig. 1 Schematic diagram of (a) current-carrying friction and wear test bench, (b) test circuit diagram, and (c) carbon pin sampling position.

properties and is widely utilized in the pantograph-catenary system of electrified railways [23], with a bulk density of 1.66 g/cm^3. It was processed into a cylindrical carbon pin with a diameter of 10 mm and a length of 30 mm. The lower sample was a copper disk sample with a radius of 98 mm made from T2 copper. Table 1 presents the mass percentages of the chemical compositions of the test materials. The contact mode between the two samples was as follows: The carbon pin sample was fixed in a fixture, making vertical contact with the high-speed rotating disk sample. With the power supply connected, the relative motion between the carbon pin and the disk was utilized to simulate the sliding contact between the carbon strips and the contact wire.

To remove the oxide layer on the sample surfaces and achieve good flatness, the contact surfaces of both the carbon pin and the copper disk were polished with sandpapers with grit sizes of 100#, 600#, 1,000#, 1,200#, and 2,000#, followed by thorough cleaning. Before each set of experiments, a micrometer with a resolution of 0.0005 mm (Sanliang 312-831, Sanliang Precision Measuring Instrument Co., Ltd., China) was used to adjust the copper disk to a horizontal position. Subsequently, pure mechanical friction was applied between the carbon pin and the copper disk at a frequency of 4 Hz until good contact was established between them. The irregularity of the contact wire can generally be represented by an ideal sine function [24, 25]. Therefore, this paper focuses on simulating periodic irregularities of the contact surface. Using a pin-on-disc tribometer, the longitudinal irregularity of the contact wire is simulated by setting the irregularity of the copper disk. The irregularities of the contact wire can be classified into several types, including large irregularities, irregular suspension point positions, and minor irregularities [22]. Among them, minor irregularities have amplitudes greater than 0.3 mm. Therefore, an irregularity amplitude of 0.4 mm is selected to study its impact on carbon strip wear.

To investigate the tribological characteristics of the pantograph-catenary contact pair under different arc intensities, the experiment was designed as a single-variable test with a copper disk irregularity of 0.4 mm and currents ranging from 0 to 80 A, simulating and detecting situations with different arc intensities caused by contact wire irregularities under actual operating conditions. As shown in Fig. 2(a), a copper foil of a certain thickness is inserted between the copper disk and the insulating base to adjust the amplitude of the disk's irregularity. To record the evolution of the arc, four positions labeled 1, 2, 3, and 4 are marked on the copper disk, with position 4 being the highest (above the inserted copper foil) and position 1 being the lowest. A micrometer was used to determine that the longitudinal displacement of the carbon pin during the rotation of the copper disk exhibited sinusoidal variation, as illustrated in Fig. 2(b). The specific experimental parameters are presented in Table 2. Each experiment was repeated at least three times to ensure the reliability of the results.

During the experiments, the frictional force and normal force were measured by a two-dimensional tangential force sensor and a normal force sensor, respectively. The instantaneous friction coefficient was obtained by dividing the real-time frictional force by the normal force, and the average friction coefficient for a single experiment was calculated as the average of the basically stable instantaneous friction coefficients after 300 cycles. The actual average friction coefficient was the mean of the results from three repeated experiments. The weight of the carbon pin was measured before and after the experiment to determine its wear loss. When the experiment lasted 9 min, an infrared thermometer (InfiRay M305, IRay Technology Co., Ltd., China) was used to measure the instantaneous temperature at the contact area between the carbon pin and the copper disk.

After the experiments, to further investigate the current-carrying wear characteristics and element distribution of the C/Cu contact pair under different currents, a high-definition camera (Zoom lens 207150282, Saike Digital Technology Development Co., Ltd., China) was used to observe the macroscopic morphology of the worn surface of the carbon pins. A scanning electron microscope (SEM; HITACHI SU8010, HITACHI, Japan) and an energy dispersive spectrometer (EDS; X-flash 6160, Bruker, USA) were employed to examine the microscopic morphology and detect the element distribution on the worn surface of the carbon sample. Additionally, a three-dimensional profiler (ZeGage™ Pro HR, Zygo Corporation, USA) was used to observe the three-dimensional morphology of the arc erosion pits on the worn surface of the carbon sample.

Table 1 Chemical compositions of the test materials (mass percentage)

Material	Cu	C	O	Fe	S	P	Ni/Sb/Pb	S/N/Cl
Copper disk	99.95%	—	0.006%	0.005%	0.005%	0.008%	Bal	—
Carbon pin	—	84.85%	10.2%	—	—	—	—	Bal

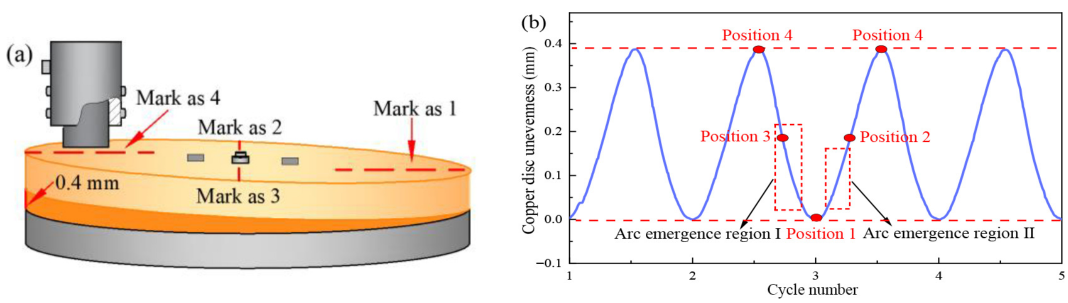

Fig. 2 (a) Copper disk irregularity setting method and (b) carbon pin longitudinal displacement diagram.

Table 2 Test parameters

Irregularity (mm)	Frequency (Hz)	Load (N)	Test time (s)	Current (A)
0.4	4	25	600	0, 25, 35, 50, 65, 80

2.2 Method for evaluating current-carrying quality

The accumulated arc energy is an important indicator for characterizing the intensity of arc burning and a crucial metric for evaluating current-carrying performance. During the experiment, the cumulative arc energy was obtained by recording the instantaneous current and voltage values through current sensors and voltage sensors. The calculation equation is shown in Eq. (1) [3]:

$$E = \int UI\mathrm{d}t \quad (1)$$

where E represents cumulative arc energy, I represents the circuit current (A), U represents the voltage drop across the carbon/copper contact interface (V), and the integration interval covers the entire experimental process.

During the process of current-carrying friction, the generation of arcs not only significantly increases material wear but also affects the conductivity of the system. In this experiment, the arc incidence rate was used to quantitatively study the frequency of arc generation under irregular operating conditions. The calculation equation is shown in Eq. (2) [26]:

$$K = \frac{\sum_{i=1}^{n} N_i \Delta t}{t} \times 100\% \quad (2)$$

where K represents the arc rate, n represents total number of arc events, i represents index variable representing the i-th arc event, N_i represents number of arc occurrences during the i-th arc event, Δt represents the duration of a single arc event, and t represents the total duration of one test.

Owing to the sensitivity limitations of the photodiode instrument, the arc rate calculated in this experiment accounts for only strong arcs, as shown in Figs. 3(a) and 3(b). Faint arcs (Fig. 3(c)) cannot be captured by the photodiode and were only recorded by a high-speed camera. Therefore, they were not included in the calculation of the arc rate.

The current-carrying efficiency is the ratio of the mean value of the dynamic current to the static current and is used to measure the system's ability to conduct current during current-carrying friction. The calculation equation is shown in Eq. (3) [6]:

$$\eta = \frac{\bar{I}}{I_0} \quad (3)$$

where η represents the current-carrying efficiency, $\bar{I}$ is the average value of the current during a single test, and I_0 is the current when the tribo-pair is stationary.

The current fluctuation reflects the magnitude of the current variation during the conduction process and is used to measure the stability of the system's electrical conduction. The calculation equation is as shown in Eq. (4) [27]:

$$S = \frac{\sum_{1}^{n} \left| I(n) - \bar{I} \right|}{\bar{I}} \quad (4)$$

where S is the fluctuation of the current-carrying current, $I(n)$ is the dynamic current value, and $\bar{I}$ is the average value of a single test current.

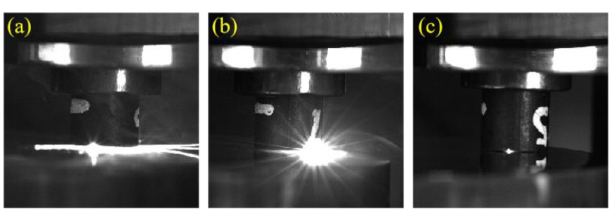

Fig. 3 Schematic diagram of (a, b) strong arcs and (c) faint arcs.

3 Results and discussion

3.1 Arc morphology

During the rotation of the copper disk, the carbon pin experiences an irregularity amplitude of 0.4 mm. When the contact voltage exceeds the breakdown voltage of this air gap, the molecules in the air are ionized into a plasma, leading to the formation of an arc [26]. Videos captured by a high-speed camera at high frame rates (Videos S1–S3 in the ESM) reveal that during the occurrence of an arc in the experiment, the detachment position of the carbon pin is indicated by the red dashed box in Fig. 2(b). Owing to the randomness of arc generation [28] and variations in current intensity, the location of arc appearance differs: When the applied current is ⩽ 50 A, arcs mostly appear near position 3 and are relatively small; when the current is ⩾ 65 A, owing to the higher intensity of the generated arcs, they occur between positions 3 and 1 (when the tribo-pair is about to separate, Region I). Additionally, arcs also appear when the carbon pin is moving from the lowest position 1 to position 2 (when the tribo-pair is about to make contact, Region II), but the intensity and duration of these arcs are significantly lower than those in Region I. Furthermore, when the current is sufficiently high, the arc column of the old arc in Region I undergoes a transition and connects with the arc root of the new arc in Region II, resulting in a continuous arc with a significantly increased duration.

The image shown in Fig. 4 captures the arc morphology recorded by a high-speed camera, depicting the approximate process of the arc from ignition to extinction under different currents. During the entire arc duration, numerous factors, such as the relative motion of the contact pair, dynamic contact pressure caused by vibration, and contact state changes, influence the arc morphology, leading to corresponding changes in the number, shape, and size of the arcs observed in the experiment. Figure 4(a) shows the arc morphology captured at 35 A. This low current level resulted in a weak arc maintenance capability. The entire arc discharge process lasts for 7 ms, with the size and intensity of the light spot reaching their maximum at 4 ms before extinguishing. When the current is 50 A, as shown in Fig. 4(b), within a complete arc duration cycle, the arc initially appears elliptical at 1 ms and diffuses by 4 ms, with the elliptical light spot visibly enlarging. Owing to the limited movement and development space for the arc column, it stretches into a long strip at 5 ms before extinguishing. The entire arc discharge process lasts for 11 ms, with the arc only appearing in Region I (Fig. 2(b)), and the arc foot position remains unchanged throughout. At 65 A (Fig. 4(c)), the duration of arc discharge significantly increases. The arc initiation stage still presents an elliptical light spot, but during subsequent development, the arc adopts an irregular shape, stretches, and emits intense arc light at 26 ms. Subsequently, the arc develops slowly and gradually weakens, slightly intensifies at 69 ms before fading away, and finally extinguishes after 102 ms. When the current reaches 80 A (Fig. 4(d)), the increased current leads to an elevation in the arc energy. Upon arc generation, its brightness and diameter continue to grow until the arc annihilates at 112 ms.

Taking the example at 65 A, the arc appears in Arc Regions I and II, as shown in Fig. 2(b), and the arc burning process undergoes stages of ignition, stable burning, diffusion, and extinction. The period from 0 to 13 ms represents the ignition stage of the arc, during which the arc develops slowly, with the contact position between the carbon pin and the copper disk being position 3. From 26 to 37 ms, the arc undergoes stable burning and diffusion. During this process, arc foot stagnation is

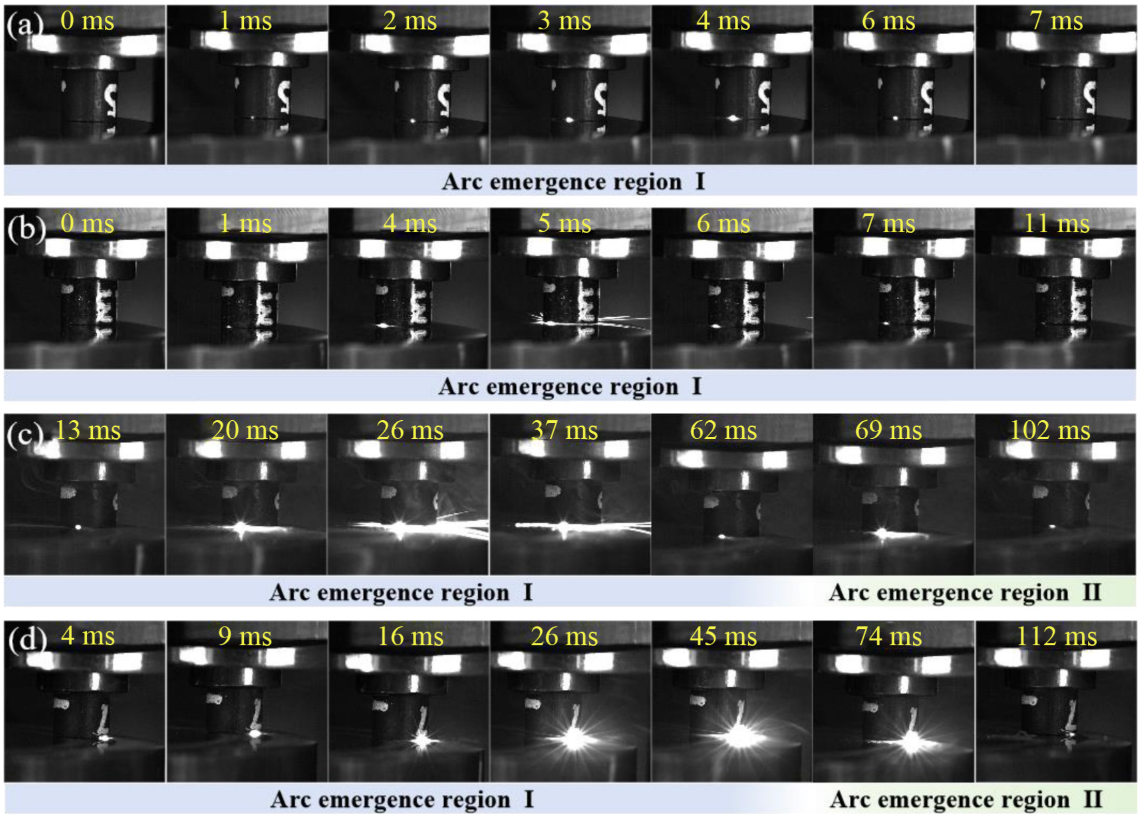

Fig. 4 Arc morphology between contact pairs under different currents: (a) 35 A, (b) 50 A, (c) 65 A, and (d) 80 A.

relatively severe, and the arc burns intensely, causing the most severe ablation of the carbon strip and the copper disk. At this stage, the contact position between the carbon pin and the copper disk is between positions 3 and 1. Subsequently, the arc gradually weakens as the contact gap continues to increase. However, when the contact point reaches position 1, the arc intensity increases slightly to 69 ms. In other words, as the contact point moves from Region I to Region II, arc foot jumping occurs, resulting in a brief interruption of the arc channel. After a new arc foot forms, the arc channel reconnects, and the arc continues. The period from 69 to 102 ms is the arc extinction stage, during which the contact position of the copper disk and the carbon pin is between positions 1 and 2. The gap between the contact pair further decreases, and the contact condition of the contact surface improves. Consequently, the brightness and radius of the arc rapidly decrease, leading to arc extinction. When the current is 80 A, the arc column of the old arc in Region I connects with the arc foot of the new arc in Region II to form a continuous arc. Throughout this process, the arc root experiences severe stagnation, which not only causes the arc to dwell on the carbon pin for an extended period but also results in slower arc stretching due to its sluggish development. This leads to a continuous expansion of the arc volume, making extinguishing and causing more severe erosion to the tribo-pair difficult.

3.2 Current-carrying performance

Figure 5 shows the variation in the arcing rate, current-carrying efficiency, and current fluctuation with current in the current-carrying system. As the current increases, the arcing rate tends to increase steadily. Within the current intensity range of 25–50 A, the current-carrying efficiency and current fluctuation remain relatively stable. Within this range, the arcing rate is very low, with only 0.78% at 25 A and increasing to just 3% even at 50 A. Therefore, most arcs occurring within the 25–50 A range are weak (Fig. 3(c)), exerting minimal influence on the current-carrying performance of the electrical circuit. When the current intensity reached 65 A, the arcing rate significantly increased. According to Fig. 4, the single arc time also increases dramatically. The generation of large arcs deteriorates the current-carrying performance, leading to a decrease in the current-carrying efficiency and an increase in current fluctuations. At 80 A, the arcing rate reaches 43.47%, but the current-carrying performance does not continue to degrade; instead, compared with the current efficiency at 65 A, it increases slightly, and the current fluctuation decreases. The relevant reasons for this are discussed in Section 3.4.

3.3 Arc energy and temperature rise

The cumulative arc energy and contact pair temperature under different currents, along with their relationships, are illustrated in Fig. 6. As the current increases from 25 to 80 A, the cumulative arc energy gradually increases from 21.58 to 130.89 kJ (Fig. 6(a)). Simultaneously, the temperature of the tribo-pairs also tends to increase, changing from 104.4 °C at 25 A to 358.6 °C at 80 A. Notably, the cumulative arc energy and contact pair temperature exhibit the same trend of change, with a gradual increase from 25 to 65 A and a significant increase from 65 to 80 A. Thus, the least squares method was used to fit the temperature and cumulative arc energy, yielding the regression equation (Eq. (5)):

$$T = 60.7 + 21.1E \tag{5}$$

where T represents the contact pair temperature in degrees Celsius, and E represents the cumulative arc energy (10^4 J).

The fitting curve is shown in Fig. 6(b). The Pearson correlation coefficient between the cumulative arc energy and temperature increase is 0.99018. A Pearson correlation coefficient value exceeding 0.8 indicates a very strong relationship between two variables [5]. Clearly, in this experiment, there is a very strong

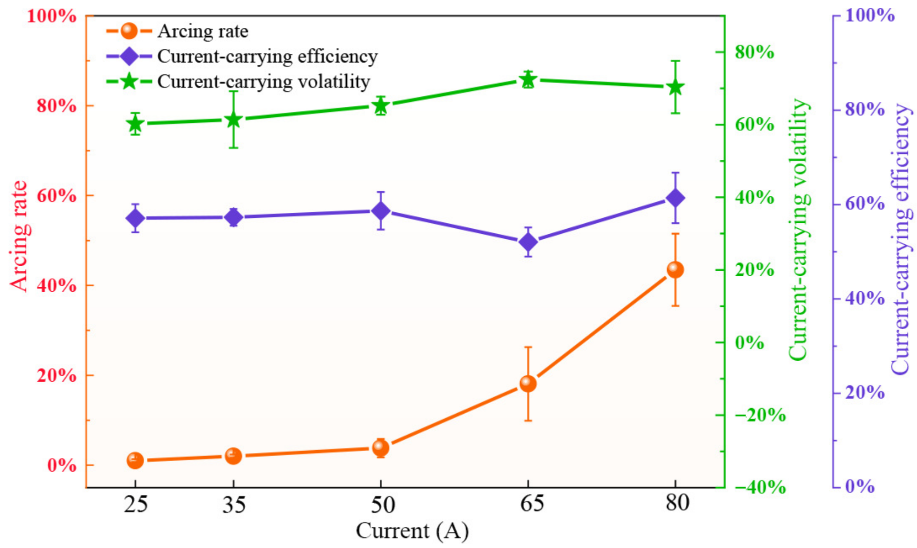

Fig. 5 Evolution of arc rate, current carrying efficiency, and current carrying stability under different currents.

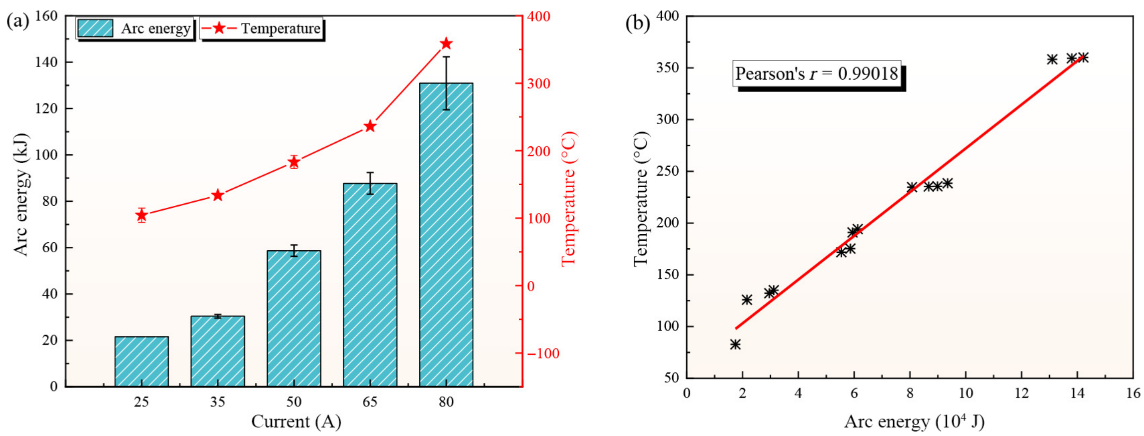

Fig. 6 Cumulative arc energy and temperature rise with (a) current variation curve and (b) linear fitting between the two.

positive correlation between the arc energy and the increase in temperature. The heat generated during the current-carrying friction process consists of three components: Joule heat, arc heat, and friction heat [26]. The above results suggest that friction heat and Joule heat have relatively minor impacts on the temperature increase compared with arc heat and that arc heat is the primary cause of the temperature increase in current-carrying tribo-pairs. When the current intensity reached 65 A, the sharp increase in temperature and arc energy led to rapid deterioration of the contact conditions on the tribo-pair surface.

3.4 Relationship between the arc intensity and current

To investigate the impact of arc discharge on current, an analysis was conducted on the current waveforms at 65 and 80 A, as well as the correlation between the current waveform and arc intensity at 80 A, as illustrated in Fig. 7. The irregularity of a copper disk results in a dynamic current waveform resembling a sine wave. In other words, when the carbon pin slides to position 4 of the copper disk (Fig. 2), the contact interface is in good contact, and the current is close to the rated current value. When the carbon pin slides to position 1, there is a gap between the carbon pin and the copper disk, and the current drops to 0, as shown in Fig. 7(a). Specifically, when the contact position between the carbon pin and the copper disk is at location 4, the measured current is approximately 60 A. As the contact position rotates to location 1, the current decreases to 0 A. At this time, the arc between the contact pairs does not affect the change in the current waveform, which is the normal current-carrying state under irregular working conditions. However, when the current reaches 80 A (Fig. 7(b)), the current does not decrease to 0 A when the carbon pin reaches the lowest position of the disk, but rather experiences current distortion.

A comparison of Figs. 7(c) and 7(d) clearly reveals that even under the same operating conditions (80 A), arc discharge has varying effects on the current waveform. When a large arc appears on the contact surface, i.e., when the arc intensity reaches its peak (Fig. 7(c)), the current undergoes corresponding distortion, manifested as a change from 35 to 75 A. This indicates that even when the contact position is at the lowest point (location 1) on the copper disk, the current remains nonzero, allowing the formation of a current loop. At this point, the existence of the arc presents a current-continuing effect [27]. As the arc intensity subsequently stabilizes at approximately 1, continuous large arcs appear, and the current remains almost stable between 60 and 75 A. Under these conditions, the arc not only causes severe arc erosion to the carbon strip and contact wire but also significantly affects the electrical performance, with the current-continuing effect of the arc becoming more pronounced. This is the primary reason why the current-carrying efficiency increases slightly with increasing arcing rate, as mentioned in Section 2.2. Conversely, when no large arc is generated between the contact pairs under 80 A conditions, i.e., when the arc intensity is 0 (Fig. 7(d)), the current no longer experiences waveform distortion and remains in a normal current-carrying state.

3.5 Friction coefficient and wear loss

The friction coefficient is a crucial parameter for characterizing the tribological and wear performance of contact pairs. Figure 8(a) depicts the evolution of the friction coefficient of the contact pair with the number of cycles under different current conditions. When no current passes through the contact pair, the friction coefficient remains stable with minimal fluctuations. However, as the current intensity increases, the fluctuation in the friction coefficient also intensifies. When the current reaches 80 A, the instantaneous friction coefficient significantly varies. This increase in friction coefficient fluctuation can be attributed to several factors. First, when the contact pair separates, the tangential force decreases or increases due to the separation and re-engagement of the contact pair, leading to fluctuations in the friction coefficient. This effect is consistent across all current intensities. Second, when the carbon pin moves to a fixed area of the copper disk, an arc forms due to the gap between the contact pairs. The presence of arc heat instantaneously increases the temperature, softening the copper disk and resulting in an abnormal increase in carbon wear debris, which further contributes to fluctuations in the friction coefficient, particularly at high currents. Additionally, as the current intensity increases, the frequency of arc occurrence increases, and the arc duration increases. The surface of the contact pair becomes rough and uneven due to arc erosion, significantly degrading the surface quality and exacerbating the fluctuation in the friction coefficient.

Figure 8(b) shows the changes in the average friction coefficient and carbon pin wear volume with current during the experiment. The average friction coefficient gradually increases with increasing current. At 0 A, the average friction coefficient is only 0.11, whereas at 80 A, it reaches 0.31. However, a lower average friction coefficient is observed at 35 A. This is because at 35 A, the arcing rate is extremely low, with only a few weak arcs appearing. Wear between the contact pairs is due primarily to cutting and scratching. The main sources of temperature rise are Joule heat generated by the current passing through the contact pair and frictional heat produced by friction. At this point, the wear debris generated by friction adheres to the wear track, and the increase in contact surface temperature accelerates the oxidation of the contact interface material, promoting the formation of an oxide layer that acts as a lubricant and reducing the friction coefficient [29]. However, when the current increases to 50 A, the surface temperature of the contact pair increases, with the arc heat becoming the primary heat source. Arc erosion and a sharp increase in temperature disrupt the oxide film on the surface, making it rough and uneven, and the average friction coefficient increases sharply.

Furthermore, as the current increases, the overall wear volume tends to increase. Without current, the wear type of the contact pair is mechanical wear, with a relatively low wear volume. When current passes through, the wear type of the contact pair includes

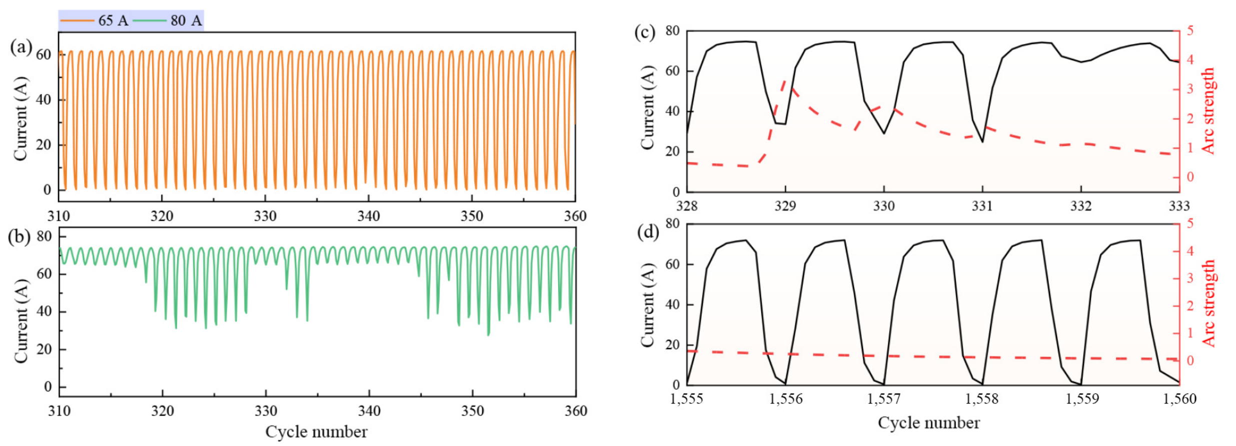

Fig. 7 Current waveform curve: (a) 65 A and (b) 80 A. The relationship between arc intensity and current under 80 A: (c) current distortion; (d) normal current.

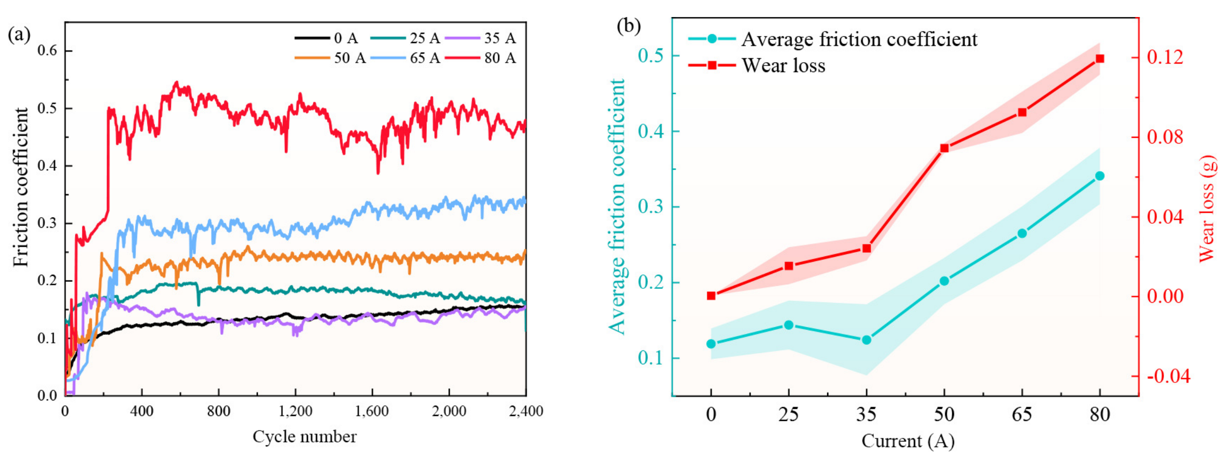

Fig. 8 (a) Friction coefficient curve between contact pairs and (b) average friction coefficient and wear amount of carbon material.

https://doi.org/10.26599/FRICT.2025.9441102

mechanical wear, electrical wear, and mechanical-electrical coupling wear [23]. As the current increases, the proportion of wear caused by electrical wear increases, and material delamination caused by arc erosion is the primary reason for the increase in wear volume [30].

3.6 Relationship between the arc intensity and friction coefficient

Figure 9(a) depicts the temporal variation curves of both the friction coefficient and the arc intensity. As illustrated, there exists a certain correspondence between the instantaneous changes in the friction coefficient of the rubbing pair and the arc intensity. Specifically, when the arc intensity sharply increases or abruptly changes, the friction coefficient gradually decreases. In other words, when intense arcing occurs between the contact pairs, as shown in Fig. 9(b), it also influences the variation in the friction coefficient. This may be attributed to the intense arcing facilitating the formation of a carbon transfer film on the contact surface, which serves as a lubricant between the interfaces. When this transfer film is subsequently disrupted, the friction coefficient increases again. Therefore, the generation of strong arcs becomes a major cause of friction coefficient fluctuations. Additionally, when significant changes in arc intensity occur, they can, to a certain extent, serve as indicators of impending changes in the friction coefficient.

3.7 Analysis of the carbon pin surface morphology

To gain a more intuitive understanding of the wear conditions of the carbon pins, Fig. 10 presents the macroscopic morphologies of the carbon pins after erosion under different current intensities. At 35 A, the carbon pin surface is characterized mainly by plowing marks, with almost no large ablation pits present. When the current increases to 50 A, obvious mechanical scratches become visible, and ablation phenomena are only observed at the edges of the carbon pin, albeit not severely. As the current continues to increase, the intensity of arc ablation also intensifies, leading to a continuous expansion in the proportion of the ablation area. When the current is less than 80 A, arc ablation primarily occurs in a small section of the carbon pin and is predominantly concentrated near the exit point along the sliding direction. This is attributed to the intensification of the arc strength when the arc is unrestrained and detaches from the contact interface. Consequently, the degree of erosion at the exit point increases drastically [28]. Furthermore, the migration behavior of arc discharge subjects the worn surface to repeated and cumulative thermal and sputtering impacts along the sliding direction, leading to a directionally intensified erosion phenomenon [31]. This erosion deteriorates the surface quality, increasing the susceptibility of this area to arc occurrence, thereby establishing a vicious cycle. However, when the current intensity reaches 80 A, owing to the immense arc strength and extremely high arcing rate (Fig. 5), the arc ablation area spreads across the entire carbon contact surface. The cumulative arc energy and arcing rate have a full impact on the tribo-pair in terms of wear morphology, and the magnitude of both directly determines the degree of ablation on the carbon pin surface.

To analyze the wear damage on the surface of the carbon pins under different current intensities, observations and analyses of the micromorphology and elemental distribution on the carbon pin surfaces were conducted, as shown in Fig. 11. When the current is less than 25 A, the worn surface is mainly distributed with plowing (Fig. 11(a2)) and debris (Fig. 11(b2)) caused by abrasive wear. At 35 A, the content of oxygen (O) on the carbon pin surface increases significantly. Combining this with the distribution of O (Fig. 11(c3)), it can be inferred that oxidation occurs on the carbon pin surface, likely forming an oxide film that acts as a lubricant, corroborating the decrease in the average friction coefficient at 35 A as mentioned in Section 2.5. The pits at

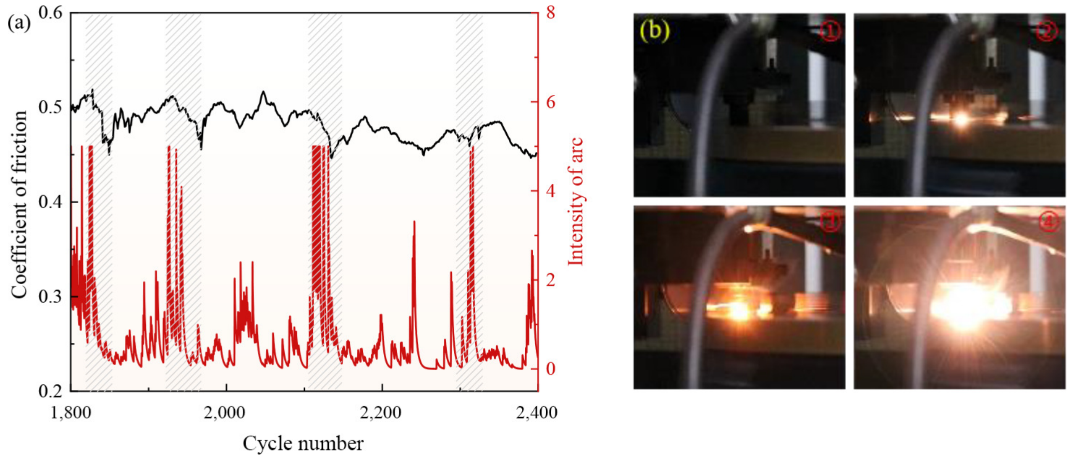

Fig. 9 (a) Relationships between the arc intensity and friction coefficient at 80 A and (b) severe arc burning images.

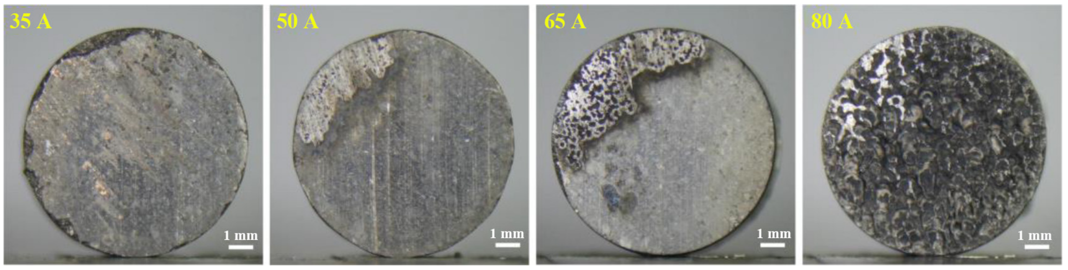

Fig. 10 Macroscopic morphology of carbon pin worn surface under different current intensities.

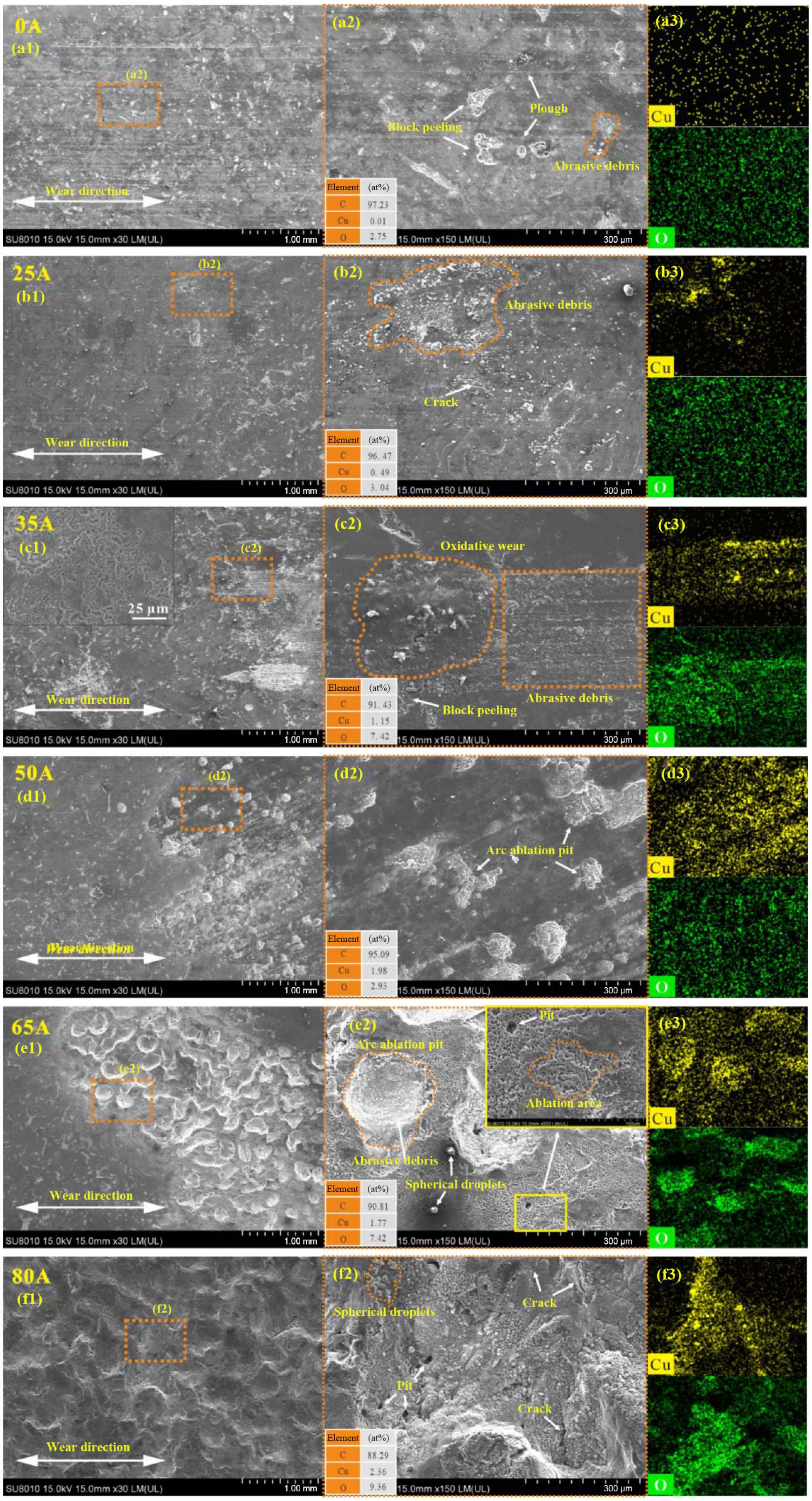

Fig. 11 Microscopic morphology and element distribution of carbon pin worn surface under different currents: (a1–a3) 0 A, (b1–b3) 25 A, (c1–c3) 35 A, (d1–d3) 50 A, (e1–e3) 65 A, and (f1–f3) 80 A.

35 A are caused mainly by delamination of the material under shear forces. Owing to the relatively small arcs generated, the arc ablation areas mostly exhibit a network-like structure, as shown in the inset of Fig. 11(c1) (since the ablation areas are small and shallow, they are not visible in Fig. 12(a)). When the current reached 50 A, arc erosion pits began to appear on the carbon pin surface. These pits are sparsely distributed (Fig. 11(d1)) and relatively shallow (Fig. 12(b)). The arc damages the material surface, making the carbon layer loose. Owing to the instantaneous temperature of arc erosion reaching 3,000–5,000 K, the carbon material undergoes gasification [32], and the countermating copper also undergoes melting and sputtering, transferring to the carbon wear surface and concentrating within the ablation pits to form numerous condensed spherical Cu particles [33]. Therefore, the primary reason for the significant increase in wear loss at a current intensity of 50 A is the material loss caused by arc erosion (Fig. 8(b)). Compared with 35 A, arc erosion is more severe, leading to fragmentation of the surface oxide film and a decrease in O content, accompanied by an increase in the average friction coefficient. At 65 A, strong arcs ablated at the same location multiple times, significantly increasing the diameter and depth of the arc erosion pits (Fig. 12(c)). The elemental analysis revealed that the erosion pits are rich in Cu and O (Fig. 11(e3)), indicating substantial melting and transfer of the countermating Cu material. The intensity of arc erosion on both carbon and copper materials increases significantly. Moreover, magnified observations of the surrounding area of the erosion pits (Fig. 11(e2)) reveal a network-like porous structure formed by the burning of the arc root, which has extremely low mechanical strength and is prone to damage and stripping during sliding contact, contributing to material loss. When the current increases to 80 A, the carbon pin surface is completely covered by erosion pits, with a diameter approximately three times greater than that at 35 A (Fig. 12(d)). Multiple cracks are scattered within the pits (Fig. 11(f2)), mainly thermal stress cracks caused by high temperatures [34]. These interwoven cracks greatly weaken the material's strength, and combined with the increasing number of porous structures, there is a constant risk of delamination. Compared with the distribution of Cu, when the current is less than 50 A, the Cu is concentrated mainly in areas with wear debris, indirectly confirming that mechanical wear is dominant below 50 A, with Cu wear occurring through plowing and transfer. At 50 A, Cu is distributed both in arc erosion pits and on the plowed surface and is not affected by arc erosion (Fig. 11(d3)), indicating that material loss is caused by the combined effects of mechanical wear and electrochemical wear. When the current exceeds 50 A, Cu is mainly concentrated in the ablation pits, accompanied by a surge in oxygen. Therefore, as the arc intensity increases, the primary form of wear on the countermating surface gradually shifts from mechanical wear to arc erosion wear, with increased Cu transfer and severe deterioration of the material surface.

Through in-depth analysis of the aforementioned results, the microscopic evolution mechanism of the wear surface of the contact pair is illustrated in Fig. 13. When the current intensity ranges from 0 to 25 A, the primary wear mechanism is abrasive wear. Abrasive debris consisting of copper and carbon appears on the contact surface, and material loss occurs through plowing and material transfer (Fig. 13(a)). As the current intensity increases to 35 A, a combination of frictional heat and Joule heat elevates the surface temperature of the contact pair, accelerating the oxidation process on the copper surface. Consequently, a dense oxide film forms on the surface, serving as a lubricant (Fig. 13(b)).

With further increases in current intensity, the arc incidence rate increases significantly, leading to severe arc erosion that cracks the oxide film (Fig. 13(c)). The proliferation of surface cracks markedly diminishes the mechanical properties of the carbon material, causing it to vaporize, sublime, and escape from the surface, thereby forming erosion pits and a porous structure. Moreover, during the arc erosion process, the copper material undergoes molten sputtering and solidifies into spherical copper particles, which are then transferred into the arc ablation pits on the worn carbon surface. Notably, the wear volume of the contact pair increases substantially, rendering the contact interface uneven and leading to a drastic deterioration in the electrical contact performance (Fig. 13(d)).

4 Conclusions

On the basis of the offline friction-induced discharge phenomenon between carbon strips and irregular Cu contact

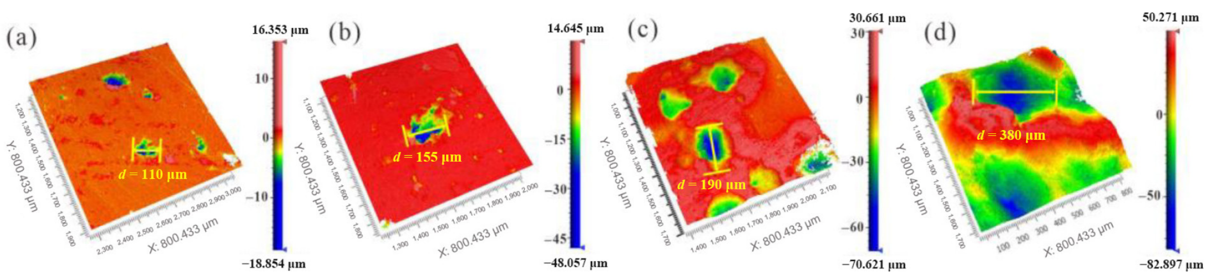

Fig. 12 Three dimensional morphology of erosion pits on the worn surface of carbon pins under different currents: (a) 35 A, (b) 50 A, (c) 65 A, and (d) 80 A.

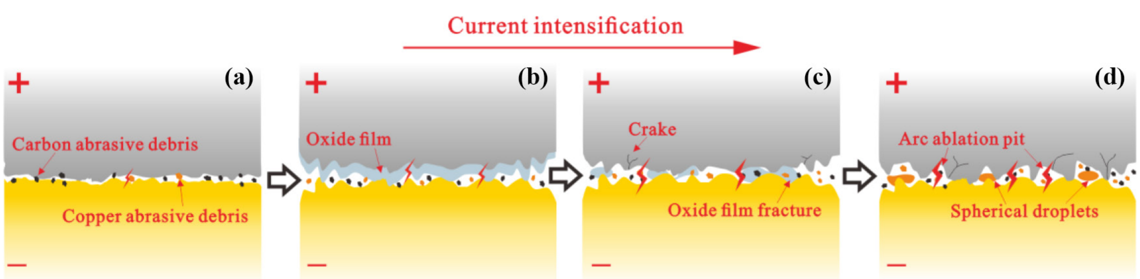

Fig. 13 Microscopic evolution mechanism diagram of worn surface of C/Cu contact pair with current variation.

wires, this paper delves into the differences in the electrical performance and friction-wear properties of the contact pair under various current intensities. The followings are the key findings:

(1) When the current reaches a sufficient level, the arc column of the old arc, which occurs when the contact pair separates, connects with the arc foot of the new arc that is yet to make contact, leading to the formation of a continuous arc. Additionally, under the same current, the arc intensity prior to contact is significantly lower than that during separation. Once the current intensity exceeds 50 A, the arc incidence rate increases dramatically, with frequent occurrence of intense arcs. Arc discharge causes varying degrees of current distortion, impacting the electrical performance of the system.

(2) The temperature, arc energy, and wear volume are positively correlated with the current intensity. However, owing to the lubricating effect of the oxide film, a turning point in the friction coefficient is observed at 35 A. Specifically, there is a direct proportional relationship between temperature (T) and cumulative arc energy (E), with $T = 60.7 + 21.1E$ and a Pearson correlation coefficient of 0.99018. The primary source of heat macroscopically is arc heat, whereas friction heat and resistance heat play only minor roles. Furthermore, the current-carrying capacity and operational stability of the system influence each other, and severe arc discharge phenomena of the contact pair can be predicted to some extent through abrupt changes in the friction coefficient.

(3) The presence of arcs not only affects electrical performance but also causes severe damage to carbon strips. The proportion of the arc erosion area, depth, and diameter of the erosion pits on the carbon strips are positively correlated with the arc intensity. Severe arc erosion can lead to severe pulverization, sublimation, and delamination of the carbon strip surface, with thermal stress cracks widespread in arc pits. Simultaneously, the Cu material undergoes molten sputtering and solidifies, mostly distributed within ablation pits, causing significant damage to the mating materials. As the current varies from 25 to 80 A, the wear mechanism gradually shifts from primarily abrasive wear to arc erosion wear.

Acknowledgements

This work was supported by the National Natural Science Foundation of China (Nos. 52365022 and 52375181), the Gan-Po Talent Support Program of Jiangxi Province (No. 20243BCE51035), the Natural Science Foundation of Jiangxi Province (Nos. 20242BAB20196 and 20224ACB204012), and the General Subject of State Key Laboratory of Performance Monitoring and Protection of Rail Transit Infrastructure (No. HJGZ2023208).

Declaration of competing interest

The authors have no competing interests to declare that are relevant to the content of this article. The author Minhao Zhu is the Editorial Board member of this journal.

Electronic Supplementary Material

Supplementary material (videos captured by a high-speed camera at high frame rates) is available in the online version of this article at https://doi.org/10.26599/FRICT.2025.9441102.

References

[1] Gao G Q, Wang Q S, Wang H, Qian P Y, Peng W, Ma Y G, Dong D L, Wang X F, He S H, Yang Z F, Wu G N. Study on current-carrying tribological characteristics of C–Cu sliding electric contacts under water accumulation from rainfall condition. *Phys Scripta* **99**(5): 055970 (2024)

[2] Liu X L, Zheng Y T, Deng G H, Xiao Q, Shen M X, Zhang D, Cao H Y, Wang Z, Gao M S, Wu H Y, Cao Y. Comparative study of the current-carrying property of different copper-impregnated carbon skateboards/contact wires. *Tribol Int* **195**: 109630 (2024)

[3] Hu Y, Huang P P, Cheng C, Zhang M M, Ma R. Influence of arc discharge on the temperature and wear behaviors of the contact strip in pantograph-rigid catenary systems under AC conditions. *Wear* **546–547**: 205368 (2024)

[4] Liu X L, Zheng Y T, Guan X, Deng G H, Xiao Q, Gao M S, Zhang D, Cao H Y, Wang Z, Cao Y, Wu H Y. An investigation revealed the influence of the different magnitude and duration of the current-impact on the wear property to the carbon skateboard/stainless steel contact. *Wear* **548–549**: 205366 (2024)

[5] Ren W J, Chen G X, Dong B J, Song Q F, Feng X H, Li L, Yang H J, He Q X. Experimental study of the effect of contact line profiles on the wear mechanism of a skateboard. *Tribol Int* **192**: 109317 (2024)

[6] Yang Z H, Song Y J, Jiao J L, Li W B, Shangguan B, Zhang Y Z. Optimization of current-carrying friction and wear properties of copper-carbon composite materials based on damage. *Tribol Int* **191**: 109074 (2024)

[7] Guo F Y, Chen M Y, Chen Z H, Shi G, Hui L C. Research on friction characteristics and modeling of pantograph-catenary sliding electrical contact. *Transactions of China Electrotechnical Society* **33**(13): 2982–2990 (2018) (in Chinese)

[8] Liu X L, Li Z H, Hu M J, Zhou C W, Xiao Q, Yang W B, Chen D Y. Research on the wear properties of carbon strips and contact wires at frigid temperatures. *Wear* **486–487**: 204122 (2021)

[9] Zhou Y K, Du M D, Zuo X. Influence of electric current on the temperature rise and wear mechanism of copper–graphite current-carrying friction pair. *J Tribol-T ASME* **144**(10): 101701 (2022)

[10] Lin Y, Li J Z, Pan J, Zhang C, Ni D R, Chen Q, Song W L, Lu J Y, Li B, Liu L. Current-carrying wear behavior and the interface evolution of the Cu/Al tribological pair. *Eng Fail Anal* **153**: 107549 (2023)

[11] Mei G M, Fu W M, Chen G X, Zhang W H. Effect of high-density current on the wear of carbon sliders against Cu–Ag wires. *Wear* **452–453**: 203275 (2020)

[12] Sunar Ö, Fletcher D, Beagles A. Laboratory assessment of ARC damage in railway overhead contact lines with a case study on copper-silver and low oxygen content copper. *IEEE T Power Deliver* **36**(5): 3074–3081 (2021)

[13] Xu Z L, Gao G Q, Wei W F, Yang Z F, Xie W H, Dong K L, Ma Y G, Yang Y, Wu G N. Characteristics of pantograph-catenary arc under low air pressure and strong airflow. *High Volt* **7**(2): 369–381 (2022)

[14] Shen M X, Ji D H, Hu Q, Xiao L, Li Q P. Current-carrying tribological behavior of C/Cu contact pairs in extreme temperature and humidity environments for railway catenary systems. *Sci China Technol Sc* **67**(8): 2537–2548 (2024)

[15] Zhou H Y, Liu Z G, Xiong J M, Duan F C. Characteristic analysis of pantograph–catenary detachment arc based on double-pantograph–catenary dynamics in electrified railways. *IET Electr Syst Tran* **12**(4): 238–250 (2022)

[16] Zhou H Y, Duan F C, Liu Z G, Chen L, Song Y, Zhang Y X. Study on electric spark discharge between pantograph and catenary in electrified railway. *IET Electr Syst Tran* **12**(2): 128–142 (2022)

[17] Luo X, Cai C, Yang H J, Mei G M, Gao C, Liu W P, Yang D S. Experimental research on the non-uniform wear of the carbon strip of the metro pantograph. *P I Mech Eng J-J Eng* **237**(10): 1943–1952 (2023)

[18] Song Y, Liu Z G, Wang H R, Zhang J, Lu X B, Duan F C. Analysis of the galloping behaviour of an electrified railway overhead contact line using the non-linear finite element method. *P I Mech Eng F-J RAI* **232**(10): 2339–2352 (2018)

[19] Huang C, Wang A B, Gu X H, Gao X G, He Y, Liu L, Gao F. High-frequency vibration analysis and optimization of irregular wear of pantograph carbon strips. *Shock Vib* **2020**: 8850079 (2020)

[20] Wu Q R, Gu X P, Ma Z Y, Wang A B. A study on the vibration characteristics and damage mechanism of pantograph strips in a railway electrification system. *Machines* **10**(8): 710 (2022)
[21] Liu X L, Zhou C W, Zhou X J, Hu M J, Wang D Y, Xiao Q, Guan X, Zhang W L, Zhang S, Xu Z B. Influence of different arc erosion durations on the wear properties of carbon skateboards/contact wires under low temperature. *Wear* **516–517**: 204600 (2023)
[22] Han Z X, Wang G L. Unevenness analysis of overhead rigid suspension catenary. *Journal of Railway Engineering Society* (4): 61–64 (2007) (in Chinese)
[23] Huang M, Yang B, Liao Z, Lv P J, Xiao S N, Yang G W, Zhu T. Research on wear of pantograph slide plate: A review. *Journal of Mechancal Engineering* **61**(08): 193–213 (2025) (in Chinese)
[24] Wang H R, Liu Z G, Song Y, Lu X B, Han Z W, Zhang J, Wang Y. Detection of contact wire irregularities using a quadratic time–frequency representation of the pantograph–catenary contact force. *IEEE T Instrum Meas* **65**(6): 1385–1397 (2016)
[25] Qin Y, Zhang Y, Cheng X Q, Jia L M, Xing Z Y. An analysis method for correlation between catenary irregularities and pantograph-catenary contact force. *J Cent South Univ* **21**(8): 3353–3360 (2014)
[26] Zhang Y Y, Li C H, Pang X J, Song C F, Ni F, Zhang Y Z. Evolution processes of the tribological properties in pantograph/catenary system affected by dynamic contact force during current-carrying sliding. *Wear* **477**: 203809 (2021)
[27] Zhang Y Z, Song K X, Du S M. *Current Carrying Tribology*. Beijing: Science Press, 2016. (in Chinese)
[28] Deng C Y, Yin J, Zhang H B, Xiong X, Wang P, Sun M, Wu X G. Dynamic variation of arc discharge and its effect on corrosion direction under current-carrying sliding. *P I Mech Eng Part J-J Eng* **233**(3): 380–392 (2019)
[29] Ji D H, Xiao L, Hu Q, Chen S Y, Li Q P, Shen M X. The effect of temperature on the current-carrying tribological behaviour of C/Cu contact pairs in high humidity environments. *Tribol Lett* **72**(2): 63 (2024)
[30] Yang H J, Wang K, Liu Y H, Fu L, Cui X L, Jiang G, Hu B. The formation of the delamination wear of the pure carbon strip and its influence on the friction and wear properties of the pantograph and catenary system. *Wear* **454–455**: 203343 (2020)
[31] Yang Z H, Zhang Y Z, Zhao F, Shangguan B. Dynamic variation of arc discharge during current-carrying sliding and its effect on directional erosion. *Tribol Int* **94**: 71–76 (2016)
[32] Hu Y, Dong B J, Huang H, Chen G X, Wu G N, Gao G Q. Experimental study on the temperature rise of a carbon strip and its influence on the wear performances of the carbon strip. *Tribology* **35**(6): 677–683 (2015) (in Chinese)
[33] Liu X L, Zhou C W, Wang D Y, Zhou X J, Hu M J, Guan X, Zhang W L, Zheng Y T, Gao M S, Yang W B, Xiao Q. Effect of arc erosion under different currents on wear mechanism of impregnated copper carbon skateboard/Cr–Zr–Cu contact wire. *Tribology* **44**(2): 189–199 (2024) (in Chinese)
[34] Wang H, Gao G Q, Wei W F, Yang Z F, Yin G F, Xie W H, He Z J, Ni Z R, Yang Y, Wu G N. Influence of the interface temperature on the damage morphology and material transfer of C–Cu sliding contact under different current amplitudes. *J Mater Sci* **57**(8): 5006–5021 (2022)

Dehui Ji received her master degree in material science and engineering in 2016 from Tianjin University, China. Since 2021, she has been pursuing a Ph.D. degree in transportation engineering at East China Jiaotong University, Nanchang, China. Her research interests cover current-carrying tribology and surface protection technology. She has published nearly 40 academic papers in SCI- and EI-indexed journals, and has undertaken one National Natural Science Foundation of China.

Mingxue Shen received his Ph.D. degree in mechanical design and theory from Southwest Jiaotong University in 2012. He has been a professor at East China Jiaotong University, China, since 2018. His current research interests include the service behavior and interface performance regulation of high-speed/heavy-haul wheel-rail systems, performance enhancement and optimal matching of rail transit braking systems, surface strengthening and life extension of critical components in advanced equipment. In recent years, he has undertaken four national-level projects, including the General Program of the National Natural Science Foundation of China. He has published nearly 100 academic papers in SCI- and EI-indexed journals and holds over 20 authorized national invention patents. He was awarded the 2022 Zhan Tianyou Railway Science and Technology Award (Special Award for Rail Transit Equipment).